

## Iron oxides in Comet 81P/Wild 2

J. C. BRIDGES<sup>1\*</sup>, M. J. BURCHELL<sup>2</sup>, H. CHANGELA<sup>1</sup>, N. J. FOSTER<sup>2</sup>, J. A. CREIGHTON<sup>2</sup>,  
 J. D. CARPENTER<sup>3</sup>, S. J. GURMAN<sup>4</sup>, I. A. FRANCHI<sup>5</sup>, and H. BUSEMANN<sup>5,6</sup>

<sup>1</sup>Department of Physics & Astronomy, Space Research Centre, University of Leicester, Leicester LE1 7RH, UK

<sup>2</sup>Centre for Astrophysics and Planetary Science, School of Physical Sciences, Univ. of Kent, Canterbury, Kent CT2 7NH, UK

<sup>3</sup>ESTEC, Keplerlaan 1, 2201 AZ Noordwijk, the Netherlands

<sup>4</sup>Department of Physics & Astronomy, University of Leicester, Leicester LE1 7RH, UK

<sup>5</sup>Planetary and Space Science Research Institute, Open University, Walton Hall, Milton Keynes MK7 6AA, UK

<sup>6</sup>School of Earth, Atmospheric and Earth Sciences, University of Manchester, Manchester M13 9PL, UK

\*Corresponding author. E-mail: [j.bridges@le.ac.uk](mailto:j.bridges@le.ac.uk)

(Received 8 December 2008; revision accepted 21 September 2009)

**Abstract**—We have used synchrotron Fe-XANES, XRS, microRaman, and SEM-TEM analyses of Stardust track 41 slice and track 121 terminal area slices to identify Fe oxide (magnetite-hematite and amorphous oxide), Fe-Ti oxide, and V-rich chromite (Fe-Cr-V-Ti-Mn oxide) grains ranging in size from 200 nm to  $\sim 10$   $\mu$ m. They co-exist with relict FeNi metal. Both Fe-XANES and microRaman analyses suggest that the FeNi metal and magnetite (Fe<sub>2</sub>O<sub>3</sub>FeO) also contain some hematite (Fe<sub>2</sub>O<sub>3</sub>). The FeNi has been partially oxidized (probably during capture), but on the basis of our experimental work with a light-gas gun and microRaman analyses, we believe that some of the magnetite-hematite mixtures may have originated on Wild 2. The terminal samples from track 121 also contain traces of sulfide and Mg-rich silicate minerals. Our results show an unequilibrated mixture of reduced and oxidized Fe-bearing minerals in the Wild 2 samples in an analogous way to mineral assemblages seen in carbonaceous chondrites and IDPs. The samples contain some evidence for terrestrial contamination, for example, occasional Zn-bearing grains and amorphous Fe oxide in track 121 for which evidence of a cometary origin is lacking.

### INTRODUCTION

Since the recovery of the Stardust capsule in January 2006, samples from the coma of Comet 81P/Wild 2 have started to reveal what this Jupiter family comet is made of (Brownlee et al. 2006). Burchell et al. (2008) estimated that approximately 1200 particles larger than 3  $\mu$ m had struck the cometary collector at 6.1 km/s. The high speed of the impact events causes some processing of the particles during capture. As discussed in Hörz et al. (2006) and Burchell et al. (2008), three types of tracks are found in the Stardust aerogel: Type A (relatively slender tracks that taper to an end where a “terminal” grain is found, which may, however, only be an unknown fraction of the originally incident particle), Type B (tracks with an initially bulbous cavity lined with fragments of the impactor and beneath which one or several slender tracks emerge, which again often con-

tain terminal grains) and Type C (tracks with just a bulbous cavity lined with fragments of the initial particle). The incident particle may thus break apart during capture and also undergo heating as it passes through the aerogel. Hence, any cometary dust grain along an aerogel track should be considered as a fragment of the originally incident dust grain (which generated that aerogel track) and which may have undergone shock and/or heat processing during capture.

In the initial description following the preliminary examination phase, Zolensky et al. (2006) described the particles captured in the aerogel as an assemblage of ferromagnesian silicates (particularly forsterite and enstatite), Fe-Ni sulfides, and Fe-Ni metal, mainly in nanometer-size grains with relatively few larger, micron-size grains that are in terminal positions within impact tracks. Similarly Hörz et al. (2006) and Kearsley et al. (2008) have shown that the Al foils that held the aerogel

1 cells in place collected a similar assemblage consisting  
2 mainly of Mg-rich silicates and abundant Fe-Ni sulfides  
3 in micron-size crater residues. Flynn et al. (2006) and  
4 Flynn (2008) used synchrotron XRF to show that the  
5 composition of the cometary material in the aerogel  
6 tracks was similar to CI chondrites to within 35–60%  
7 for the major elements but with more variance for the  
8 moderately volatile elements which they showed were  
9 similar to anhydrous porous interplanetary dust parti-  
10 cles (IDPs). The presence of refractory material and  
11 possibly chondrule fragments has been taken to indicate  
12 mixing between material formed in the inner Solar Sys-  
13 tem and less refractory material that constitutes the  
14 bulk of comet Wild 2 (Brownlee et al. 2006; Nakamura  
15 et al. 2008). However, hydrous phases such as serpen-  
16 tine or phases precipitated from hydrothermal fluids are  
17 notably absent from the reported comet Wild 2 inven-  
18 tory and this is unexpected because chondrites and IDPs  
19 carry widespread evidence for hydrothermal action.

20 The Wild 2 results show similarities with known  
21 extraterrestrial materials, but there are also differences.  
22 Ishii et al. (2008) reviewed the mineralogical work car-  
23 ried out on comet Wild 2 to date and suggested that  
24 there were stronger similarities to asteroidal meteorites  
25 than to IDPs. Until the Stardust mission, IDPs have  
26 been our only source of cometary material (Rietmeijer  
27 1998). Westphal et al. (2008) used X-ray absorption  
28 data (Fe-XANES) to show that Wild 2 tracks have a  
29 mixture of oxidized and reduced Fe that is broadly con-  
30 sistent with chondrite-like compositions but not clearly  
31 linked to any one known chondrite group. Joswiak  
32 et al. (2008) have shown the presence of Na-rich pyrox-  
33 enes in 15 tracks, also with compositions distinct from  
34 those of known unequilibrated chondrites. Thus, the  
35 diversity of mineralogical assemblages present in comets  
36 is becoming apparent. GEMS (Glass with Embedded  
37 Metal and Sulfide), components that are characteristic  
38 of IDPs have also not been firmly identified or distin-  
39 **4** guished from molten aerogel (Zolensky et al. 2007).

40 Detailed mineralogical studies of the cometary  
41 grains distributed along the aerogel tracks (as distinct  
42 from terminal grains at the ends of tracks) have shown  
43 the importance of understanding the effects of collection  
44 such as heating and oxidation or reduction within the  
45 aerogel at 6.1 km/s. This is discussed in more detail in  
46 Grosse et al. (2008) and Burchell and Kearsley  
47 (2009) and Burchell et al. (2006a). Briefly, Rietmeijer  
48 et al. (2008) and Leroux et al. (2008) used analytical  
49 TEM analyses of samples from along cometary tracks  
50 to show that the most frequent microstructure consists  
51 of a silica-rich glassy matrix containing a large number  
52 of vesicles and abundant Fe-Ni-S inclusions. This sug-  
53 gests that a large proportion of incoming dust particles  
54 were fully melted and mixed with molten aerogel. The

larger particles toward the terminal ends of the aerogel  
tracks have preserved more of the pristine cometary  
material. This is in agreement with studies of laboratory  
analog samples where mineral projectile grains of  
known composition were captured in aerogel using  
light-gas gun experiments (e.g., Noguchi et al. 2007;  
Hörz et al. 2008; Burchell et al. 2009).

In this article, we report on analysis of grains found  
in two tracks in the Stardust aerogel (both grains  
located along track walls and terminal grains). A variety  
of complementary analysis techniques have been used  
i.e., optical microscopy, SEM, microRaman, micro XRS  
fluorescence, and Fe-XANES, EXAFS. The focus of  
our work has been the identification of oxide phases in  
the samples and consideration of their possible origins.

## SAMPLES AND METHODS

The track 41 keystone (from C2044,0,41,0,0) was  
cut and prepared at the University of California (Berke-  
ley) (using the method described in Westphal et al.  
2002). In the nomenclature of Hörz et al. (2006) and  
Burchell et al. (2008), track 41 is a Type B, “turnip”  
shaped track, where the particle has broken up during  
impact, producing a large cavity (lined with fine frag-  
ments of the impactor) in the upper half of the track.  
This cavity is accompanied by two styli, which emerge  
beneath the cavity, well aligned with the incident impact  
direction; terminal grains can be found at the end of  
these styli. The sample used here was a  $4 \times 2.5$  mm  
transverse slice through the track, close (0.8 mm) to the  
track entrance (Fig. 1) and as such was a sample of  
cometary grains distributed along a track. The aerogel  
slice was placed between two glass slides with a depres-  
sion within which the aerogel slice laid. An optical  
image of part of the aerogel slice, showing one of the  
several captured grains, is shown in Fig. 2.

Track 121 is shown in Fig. 3 and is a Type A, “car-  
rot” shaped track. Track 121 was recovered from a chip  
that fell off C2005 during the tile removal process.  
There appears to have been relatively little initial disag-  
gregation of the incident particle during capture in the  
coma and terminal grains are present at the end of the  
track. Gold mounts for the terminal particles from track  
121 were prepared at the Open University (UK).  
These were sent to NASA-JSC and microtomed  
sections of track 121 samples (C2005,2,121,1,0 and  
C2005,2,121,2,0) placed onto the Au mounts and  
returned to the UK for analysis.

In parallel to the Stardust samples, laboratory ana-  
log samples were prepared using the two stage light-gas  
gun at the University of Kent. This gun (Burchell et al.  
1999) was used to fire samples of mineral grains of  
known composition at standard aerogel samples. Unlike



Fig. 1. Track 41. This is a Type B “turnip” shaped track of length  $\sim 4$  mm and the impact was from the left of the image moving right. It was removed from the cometary collector cell 44. (See Burchell et al. 2008 for a discussion of track nomenclature and the distribution of tracks in the collector tray. An extended discussion of the characteristics of Type B tracks is given in Trigo-Rodriguez et al. 2008.). Our slice was cut 0.8 mm in (gray vertical rectangle) from the track entrance. Track image courtesy of NASA-JSC. 14

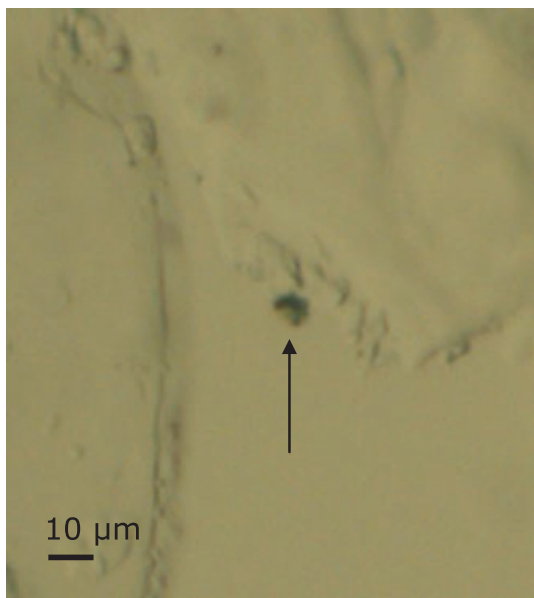


Fig. 2. Optical image of selected region of C2044,0,41 (transverse slice from track 41, see Fig. 1; also arrowed in the area Rm in Figure 11a). Shown arrowed is a grain captured in the aerogel on the wall of the track cavity (the bottom right quadrant of the figure is the track cavity, the other three quadrants are part of the extracted aerogel slice).

the Stardust aerogel (3 cm deep blocks, some of which had a density which varied from  $5 \text{ kg/m}^3$  at the front face to  $50 \text{ kg/m}^3$  at the rear surface; other cells had no significant density gradient), these laboratory samples all had a fixed density ( $27\text{--}30 \text{ kg/m}^3$ ) throughout which was chosen to be similar to the nominal Stardust density gradient. Minerals used were hematite and magnetite. Details of the samples are given in Table 1.

The analyses were planned to minimize the effects of sample damage on our mineralogical characterization. Reflected light photography and MicroRaman analyses were performed before our SEM analyses and synchrotron work. Track 41 was analyzed by microR-

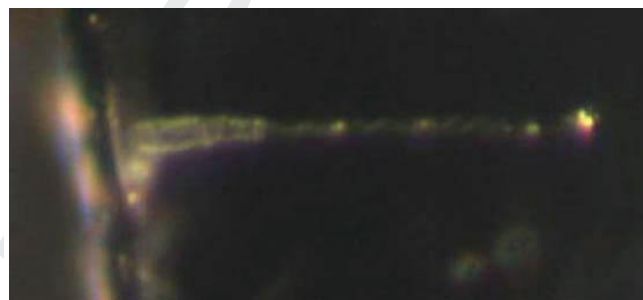


Fig. 3. Track 121. This is a Type A “carrot” shaped track of length  $\sim 0.9$  mm and the impact was from the left of the image moving right. It was taken from a chip off the cometary collector cell 5. The terminal grains used here were removed from the end of the track (bright region at right hand side of image). Image courtesy of NASA-JSC. 15

Table 1. Analog aerogel samples used in this work.

Mineral	Grain size ( $\mu\text{m}$ )	Aerogel density ( $\text{kg/m}^3$ )	Impact speed ( $\text{km/s}$ )
Hematite (Kent sample)	10	32	6.17
Magnetite (BM-2005 M316)	10	27	5.94

aman and synchrotron radiation, the track 121 terminal samples by microRaman then SEM.

### Raman Analyses at Kent and Open University

The use of Raman spectroscopy to successfully identify mineral grains captured in aerogel was demonstrated by Burchell et al. (2001) for olivine and enstatite. Subsequent work showed that a wide range of minerals could be identified with grain sizes down to  $5 \mu\text{m}$  (Burchell et al. 2006b). Once a Raman wavenumber spectrum has been obtained (and the slowly varying broad background subtracted where necessary), the remaining relatively narrow peaks can be used to identify minerals. In

1 this work, a point Raman spectrometer was used at the  
2 University of Kent to study C2044,0,41,0,0 and  
3 C2005,2,121,2,0.

4 The Kent microRaman system was integrated into  
5 an Olympus BX40 microscope. The Raman module was  
6 a Jobin Yvon microRaman module, with a HR640 spec-  
7 trograph with a CCD (liquid nitrogen cooled). Disper-  
8 sion on the CCD was about 0.5/cm per pixel. The  
9 illumination was from a He-Ne laser (632.8 nm). The  
10 full width of the laser spot size was about 3–5  $\mu\text{m}$  and  
11 the maximum laser power at the sample was about  
12 10 mW. Such a power density can be sufficient to  
13 induce significantly elevated temperatures in samples  
14 unless the heat can be conducted away efficiently.

15 Aerogel is a poor heat conductor, so care has to be  
16 taken to avoid excessive heating effects from laser illu-  
17 mination when examining small particles captured in  
18 aerogel, using laser illumination at  $\sim 750 \text{ W/mm}^2$  maxi-  
19 mum power. This is discussed in Burchell et al. (2006b)  
20 where, using the same microRaman system as here, ele-  
21 vated temperatures of typically 100–160  $^{\circ}\text{C}$  were found  
22 for small (10–50  $\mu\text{m}$ ) mineral grains captured in aerogel.  
23 These results were found to depend on the absorption  
24 power of the minerals. Olivine showed modest (20  $^{\circ}\text{C}$ )  
25 increases in temperature during laser illumination, sili-  
26 con carbide had a greater temperature (180  $^{\circ}\text{C}$ ) and one  
27 initially unknown mineral grain (subsequently identified  
28 as vanadium pentoxide by comparison with similar  
29 spectra in the literature, e.g., Zhou and He 2008) gave a  
30 temperature of 480  $^{\circ}\text{C}$ . These temperatures were esti-  
31 mated from Stokes-anti-Stokes line ratios in the Raman  
32 shift spectra. For particles, which fluoresce, higher tem-  
33 peratures were found on average. For example, ruby  
34 grains in aerogel showed temperatures of typically 20 to  
35 230  $^{\circ}\text{C}$ , while one grain (out of 15) had an elevated tem-  
36 perature under full laser illumination of  $\sim 700 \text{ }^{\circ}\text{C}$ , thus  
37 showing that, even in a sample of one material, small  
38 variations in composition or conditions inside the aere-  
39 gel can result in substantial changes in heating under  
40 laser illumination. Bearing these effects in mind, a series  
41 of filters were used to attenuate the laser illumination  
42 during the analysis. The lowest filter had only 8% trans-  
43 mission at the laser wavelength, and all analysis com-  
44 menced with this in use. Sample temperature was  
45 monitored by using ratios of Stokes and anti-Stokes  
46 lines as described previously (Burchell et al. 2006b).  
47 When analyzing Raman spectra, fitting was performed  
48 using the GRAMS/32 (Galactic) package with an  
49 assumed Lorentzian line-shape for each peak.

50 Laser Raman microprobe analyses of particle  
51 C2005,2,121,1,0 were performed at the Open University.  
52 Integration times of a few minutes using a 60  $\mu\text{W}$ , 514-  
53 nm laser, and a 1.5-micron spot resolution were  
54 employed. This gave 24  $\text{W/mm}^2$  power density, which

owing to the relatively short integration times e.g., com-  
pared with some of our other Raman analyses, mini-  
mized the risk of sample damage.

### SEM Analyses

Following the microRaman analyses, the track 121  
terminal samples were studied with an FEI Sirion Field  
Emission Gun SEM (FEG-SEM) and a Philips XL30  
Environmental SEM at UL. The FEG-SEM was oper-  
ated at 4–9 keV and a beam current of 400 pA for  
imaging. Qualitative EDS point analyses were per-  
formed at 12.5–15 keV,  $\leq 650 \text{ pA}$  beam current with a  
PGT EDS system on the FEG-SEM. Beam currents  
were measured on a Faraday cup. The ESEM (with  
Link EDS) was used at 1 torr pressure when sample  
charging on C2005,2,121,2,0 occurred during some anal-  
yses using the FEG-SEM. This was found to overcome  
the majority of charging problems. EDS analysis times  
ranged from 50–1000 s for point analyses depending on  
our assessment of sample charging, potential damage,  
and elemental concentrations. For C2005,2,121,2,0 indi-  
vidual spectrum X-ray counts from across the sample  
were added together to produce a representative spec-  
trum.

### FIB & TEM Analysis

After identification by SEM of iron oxide grains  
within a terminal area of Track 121 (C2005,2,121,2,0), a  
technique was developed for extraction of one of the  
grains for TEM analysis. An FEI Quanta 3-D Focused  
Ion Beam Scanning Electron Microscope (FIB-SEM)  
was used at UL for sample preparation: milling an  
approximately 120 nm thick wafer containing a cross  
section of one of the iron oxide grains. The FIB-SEM  
 $\text{Ga}^+$  ion beam used for the milling was operated at  
30 kV accelerating voltage. Prior to application of the  
run script, the particle was capped with a  $10 \times 2.5 \mu\text{m}$   
carbon layer approximately 150 nm thick followed by  
Pt of equivalent dimensions in order to protect the Fe  
oxide grain from the effects of the ion beam. Both lay-  
ers were deposited via electron beam deposition using  
the Gas Injection System (GIS). The conventional  
 $15 \times 4 \mu\text{m}$  TEM runscript was amended to produce a  
 $5 \times 4 \mu\text{m}$  sample wafer dimensions required miniaturisa-  
tion in order to preserve the rest of the terminal mass.  
A 120-nm thick wafer was produced to ensure that the  
particle cross section would remain intact. The wafers  
were imaged with secondary electron snap shots at  
sequential stages of the milling process and the runscript  
was aborted before the final milling currents in order to  
help preserve the wafer. Manual thinning was applied  
post extraction with low beam currents  $< 100 \text{ pA}$  to

1 ensure electron transparency of the grain. The wafer  
2 was extracted in situ using the Omniprobe lift out mech-  
3 anism, and attached to a copper grid using carbon weld-  
4 ing with the GIS and ion beam at 20 kV.

5 A JEOL 1200 TEM with a PGT EDS system was  
6 used for analysis of the extracted grain. Its LaB<sub>6</sub> therm-  
7 ionic source was operated at 200 kV and 111  $\mu$ A emis-  
8 sion current. Bright field imaging, STEM EDS, and  
9 Selected Area Electron Diffraction (SAED) were per-  
10 formed on the particle and surrounding gold foil mount.  
11 STEM EDS analyses were performed at 14 points in  
12 and around the iron oxide grain for 50 s each and X-  
13 ray mapping was performed with STEM mode for 2 h.

14 In order to check that the Ga<sup>+</sup> ions in the FIB did  
15 not create amorphous Fe oxides, we conducted FIB-  
16 SEM analyses of magnetite-bearing symplectites in  
17 nakhlite meteorites (Changela and Bridges 2009). The  
18 preservation of the magnetite and other phases showed  
19 that FIB-SEM analyses did not change the structure of  
20 the FeO studied in our Stardust samples.

## 22 MicroFocus XRS, XANES & EXAFS

23  
24 Microfocus XRS and XANES spectroscopy was  
25 performed at Beamline I18 of the Diamond Light  
26 Source, Oxfordshire. This beamline operates from a  
27 3 GeV synchrotron with typical currents of 200 mA. A  
28 Si (1 1 1) and (3 1 1) double crystal monochromator  
29 was used for energy selection with resolutions of 10<sup>-4</sup>  
30 and 10<sup>-5</sup>, respectively. A 9 element germanium based  
31 solid state detector was used which is capable of mea-  
32 suring the X-rays of Ca upwards. Energy calibrations  
33 are regularly checked on I18 with Mn metal samples.

34 Microfocus XRS (fluorescence) maps were gener-  
35 ated at 3 areas of the transverse slice of track 41  
36 (C2044, 10, 41, 0, 0). The germanium fluorescence detec-  
37 tor was placed 45° to the sample with the beryllium win-  
38 dows as close as possible to maximize count rates.  
39 250 × 250  $\mu$ m maps were produced at 13 keV and a  
40 dwell time of 5 s. Beam spot sizes were 3–4  $\mu$ m. Long  
41 integration times of 500 s were performed on hotspots  
42 identified after mapping. At characteristic energies,  
43 called absorption edges, the X-ray absorption of an ele-  
44 ment changes markedly. Near an absorption edge, the  
45 spectra may contain fine structure that reveals informa-  
46 tion about valency, the electronic and geometrical  
47 environment of the absorbing atom. Fe K edge XANES  
48 (X-ray Absorption Near Edge Structure) was performed  
49 on hotspots. Approximately 120 data points were inte-  
50 grated across the XANES pre and post Fe edge. One  
51 second integration was performed at each 0.2–0.4 eV  
52 energy step from 6962–7090 eV, followed by 5 s  
53 onwards beyond the Fe K edge (EXAFS Extended  
54 X-ray Absorption Fine Structure) up to 7500 eV. How-

ever, this region was too noisy for successful fitting to  
the co-ordination environment for track 41 and so our  
mineral identifications are based on XANES. A range  
of mineral standards similar to the phases studied were  
also analyzed: magnetite (Fe<sub>2</sub>O<sub>3</sub>FeO), hematite (Fe<sub>2</sub>O<sub>3</sub>),  
Mg-rich olivine from the Admire pallasite meteorite  
(Mg/Mg + Fe atomic ratio 0.88), chromite FeCr<sub>2</sub>O<sub>4</sub>, Fe-  
sulfide – pyrrhotite (Fe<sub>1-x</sub>S). They were powdered with  
an agate mortar and pestle and mixed with boron  
nitride powder at 5 mg to 95 mg proportions, the pellets  
were then used for XANES. Samples and standard pow-  
ders were mounted on low X-ray absorption tape to  
preserve their integrity and using this tape, together  
with the thin aerogel within which the cometary tracks  
lie, means that X-ray absorption effects for elements  
with Z  $\geq$  Ca were small enough to ignore in this work.  
XANES spectra were reduced using *Pyspline* software, 8  
XRS data with *PyMCA* software. The resultant  
XANES spectra were normalized by the software to the  
EXAFS region. The Berkeley XANES spectral library  
was also used to compare with our XANES results.

## RESULTS

### SEM and TEM of Terminal Areas of Track 121

#### C2005,2,121,1,0

This sample consists of a 10 × 10  $\mu$ m mixture of  
glassy aerogel and a few percent of cometary grains.  
The relatively smooth surface texture and compositional  
analyses suggest that this part of track 121 has under-  
gone some melting during capture heating. Spot analy-  
ses showed that there is a high concentration of iron  
oxide grains (Fig. 4). These appear to be pure Fe oxide, 9  
despite long acquisition times on numerous spots most  
grains had no other detectable elements except Fe, O  
with Au, Al, Si resulting from the substrate and aerogel.  
As some glassy aerogel was attached to the iron oxides,  
grain sizes were difficult to measure accurately but ran-  
ged up to approximately 100–200 nm. A second elemen-  
tal signature for some grains was Mg-Fe-O-(Si),  
consistent with the common presence of forsterite oliv-  
ine in many of the Stardust samples and characteristic  
of silica-rich glass in the Stardust samples (Zolensky  
et al. 2006; Leroux et al. 2008; Rietmeijer et al. 2008).

Following SEM characterisation, an Fe oxide grain  
was extracted from this sample by FIB-SEM (see the  
section FIB & TEM Analysis) and analyzed by TEM  
(Fig. 4) in order to check its composition and determine  
its structure. Figure 4d shows an EDS spectrum taken  
from the grain. The Ga peak arises from some implanta-  
tion during the ion milling process, the Au peak is  
due to excitation of some X-rays from the underlying  
mount.

Fig. 4. (a) SE image of terminal area of sample C2005,2,121,1,0 at 5 kV. Iron oxide (grains arrowed) has been found within and beside the terminal area of aerogel. Scale bar is 5  $\mu\text{m}$ . (b) SEM image of terminal area of C2005,2,121,2,0 at 9 kV. Scale bar is 5  $\mu\text{m}$ . MicroRaman spectroscopy suggests the presence of magnetite-hematite (c) SEM EDX spectra of iron oxide grain in C2005,2,121,1,0. The Au peak is from the substrate on which the particle was pressed. (d) 50 s integrated EDS spectra of an iron oxide grain in TEM after FIB extraction from C2005,2,121,1,0. (e) STEM bright field image of wafer containing Fe oxide. Scale bar is 0.2  $\mu\text{m}$ . (f) EDS Fe K $\alpha$  intensity map showing the location of the Fe-oxide, scale bar is 0.2  $\mu\text{m}$  same field of view as (e).

Selected Area Electron Diffraction of the Fe oxide grains showed the absence of any diffraction pattern and thus the oxide is structureless. The surrounding gold foil did, however, show diffraction demonstrating that it is the amorphous nature of the Fe oxide rather than the thickness of the extracted wafer that caused the lack of a diffraction pattern.

#### C2005,2,121,2,0

This sample consists of a  $6 \times 4 \mu\text{m}$  aggregate of aerogel and scattered cometary grains. Like the 121,1,0 sample it contained a dominant Fe signature (associated with iron oxide – see the Raman section below) from the cometary grains in addition to Si which is mainly produced from the aerogel (Fig. 4). However, the surrounding aerogel precluded imaging discrete grains. Subtracting the Au background from an X-ray spectra taken from the sample indicates, qualitatively, that it contains S as well as Fe and Mg. This suggests the presence of minor sulfides, although these have not been detected by microRaman, perhaps because of their small total volume. Such sub-micron grains could be fragments that were stripped off larger grains during capture. Unlike 121,1,0, this sample does not appear to have undergone melting.

Both 121,1,0 and 121,2,0 are samples of the terminal areas and thus iron oxides are present near the end of this track. A large single terminal grain has not been identified in these samples.

#### Raman

Raman analysis of the Stardust samples was carried out in addition to tests of standard sample materials.

#### Laboratory analog samples

Before considering the Stardust samples, the general case of magnetite ( $\text{Fe}_3\text{O}_4$ ) and hematite ( $\alpha\text{-Fe}_2\text{O}_3$ ) under

Raman analysis was considered. The Raman spectra of these minerals are distinct from other Fe oxides e.g., goethite and maghemite. Raman spectra were taken from raw grains of both magnetite and hematite (placed on microscope slides) using an 8% transmission filter to keep laser power on the samples low, see Fig. 5. The spectra obtained are typical of the spectra found in the literature for these minerals, e.g., de Faria et al. (1997) and the position and width of each peak are given in Table 2. For the hematite specimen (Kent microRaman), the series of seven sharp peaks, which extend up to 611/cm (what appears in the figure as a single peak at 293/cm is resolved by the fit into two narrow, just separable peaks), are similar to those reported in the literature typical of hematite and are typically assigned to the expected seven phonon lines for this material (e.g., see de Faria et al. 1997). The very weak peak at 661/cm is barely evident but is included for completeness. The peak at 1317/cm is also seen by other workers. It has been assigned to two-magnon scattering in

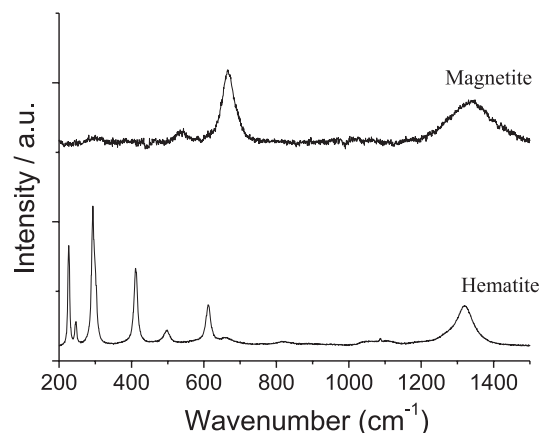


Fig. 5. Raman spectrum from raw grains of hematite and magnetite standards.

Table 2. Position and width of peaks in Raman shift spectra for samples in Table 1 and for laser heated magnetite.

Sample	Peak positions and width (/cm)	
	Raw grain	After capture in aerogel
Hematite	226.1, 4.9	218.9, 9.9
	245.9, 4.9	234.4, 6.6
	292.7, 7.2	282.9, 21.5
	299.8, 8.2	—
	411.4, 10.8	395.7, 22.8
	496.1, 19.3	478.3, 15.9
	611.7, 15.3	602.6, 51.9
	661.0, 28.7	665.6, 66.6
	1316.9, 56.9	1293.9, 79.0
	1337.0, 136.4	—
Magnetite	536.9, 27.4	—
	667.2, 39.3	661.2, 45.0
Magnetite (laser heated)	1337.0, 136.4	1323.6, 87.7
	226.0, 5.6	—
	245.2, 5.7	—
	292.1, 8.0	—
	299.4, 8.8	—
	410.5, 12.6	—
	495.8, 22.4	—
	610.8, 16.4	—
660.5, 29.4	—	
1316.4, 77.5	—	

the anti-ferromagnetic hematite (Martin et al. 1977), or more recently to an overtone of a Raman-inactive phonon (Massey et al. 1990). The magnetite spectra seen here is characterized by just two narrow sharp peaks (537 and 667/cm) and a broad peak at 1337/cm. There is some discussion in the literature (e.g., de Faria et al. 1997) as to whether the latter peak is in fact associated with magnetite or represents the presence of hematite contaminants in the samples. Here we find that it has a different peak position and width to the peak seen in the hematite at 1317/cm.

As has been pointed out by several authors (e.g., de Faria et al. 1997; Shebanova and Lazor 2003) that laser heating of magnetite samples (to 240 °C) during Raman analysis causes the appearance of bands in the Raman spectra that are associated with hematite, reflecting an irreversible temperature induced transition from magnetite to hematite at around 240 °C. This is illustrated here in Fig. 6 where 88% of full laser power (i.e., 8.8 mW) was used to heat a magnetite sample to  $205 \pm 20$  °C and take Raman spectra from it (peak positions and widths are given in Table 2). In the Raman spectrum from the heated sample, the characteristic bands of hematite at low wave shift number are now apparent, along with (and stronger than) those for magnetite. At  $\sim 1300$ /cm, the peak observed in the

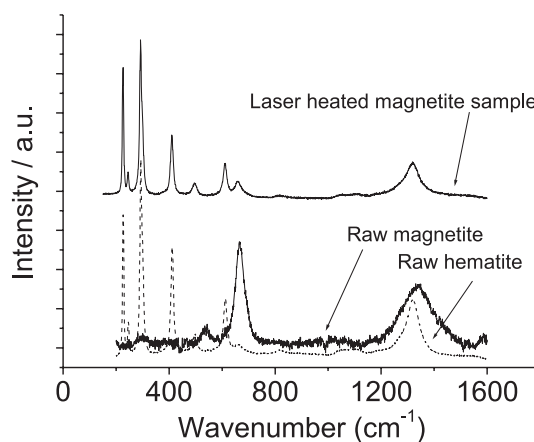


Fig. 6. Raman spectrum (upper trace) from a raw grain of magnetite illuminated at high laser power (i.e., heated to high temperature). The two lower traces are for raw grains of magnetite (solid line) and hematite (dashed line) taken at low laser power. The upper trace (peak positions and widths are given in Table 2) can be seen to be a combination of the two lower traces, with the hematite contribution dominating.

hematite sample has now replaced the broader and slightly higher wave number peak in the original magnetite spectrum (Fig. 5). This indicates that the grain has been heat processed by the laser during Raman analysis and (at the particle's surface) is now a mixture of hematite and magnetite.

This raises issues with regard to heating during analysis. Firstly, does heating during capture in aerogel alter the samples? As discussed later, there is evidence that peak projectile temperatures during capture in aerogel can reach as high as 2040 °C. In addition, Noguchi et al. (2007) report elevated temperatures, and made TEM observations of mineralogical changes in samples captured in aerogel which are associated with transition temperatures of 500 °C (i.e., in excess of those needed for the magnetite to hematite transition at low oxygen fugacities). These elevated temperatures were found in a surface layer 1–2  $\mu\text{m}$  thick of captured grains, whose interiors showed significantly less heating. Secondly, we must also consider that, even when low laser power is used, the heating effects due to the Raman laser illumination may be exacerbated for small grains captured in aerogel due to aerogel's poor heat conduction properties (particularly for long integration times).

Raman spectra were obtained at low laser power (i.e., with the 8% transmission filter) from the mineral grains captured in the laboratory aerogel samples described in Table 1, Fig. 7. For magnetite (Fig. 7a), it can be seen (Table 2) that the main characteristic peak is shifted in position by 6/cm. The broad peak at 1324/cm is barely above the noise in the spectra and by

itself would probably not trigger a peak identification. The increased signal to noise ratio in the spectra is due to the grains being observed through a thickness of aerogel (2 mm in this case, much greater than the Stardust sample analyzed below) and this is common in Raman studies of grains in aerogel. For the hematite sample, the characteristic peaks are still strongly visible after capture, albeit again with an apparent slight downward shift in peak position and increased widths (similar shifts and broadening have been reported previously when samples are heated e.g., see Shebanova and Lazor 2003). This increased width explains the inability to resolve clearly the two peaks expected at 293 and 299/cm and their appearance as a single peak. The grains used in taking these spectra were 10  $\mu\text{m}$  in size, similar within a factor of 2 to the Stardust grains that were analyzed e.g., Fig. 2. The important conclusions of these experiments are that the acquisition of Raman

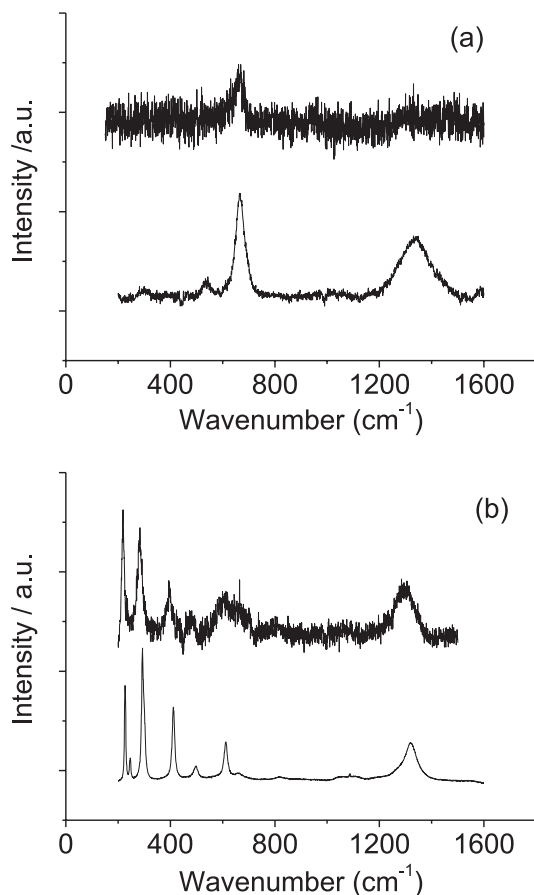


Fig. 7. Raman spectra of (a) 10  $\mu\text{m}$  magnetite and (b) 10  $\mu\text{m}$  hematite grain after capture in aerogel (density 30  $\text{kg}/\text{m}^3$ ) at 6.1 km/s. In each case, the upper spectrum is in aerogel and the lower trace is from a raw grain for comparison; the characteristic peaks of each raw sample are still present after capture (and are listed in Table 2).

spectra does not thermally process iron oxide grains sufficiently to entirely change magnetite into hematite.

As a further check, Raman spectra were taken for long (20 h) periods, at full laser power (10 mW) on magnetite grains captured in aerogel. Grains about 30  $\mu\text{m}$  in size were chosen which were near the surface of the aerogel and which were about 30  $\mu\text{m}$  in size. These laser illumination conditions exceeded those used to analyze any of the comet Wild 2 samples. The resulting Raman wave shift spectra are shown in Fig. 8. A range of results is apparent. In one case (Fig. 8a), the spectrum was altered, such that it was dominated by the peaks expected from hematite, with only weak magnetite peaks remaining. In the other case (Fig. 8b), the spectrum was still dominated by the peaks associated with magnetite. Based on ratios of anti-Stokes and Stokes lines in the Raman spectra, we associate a temperature of  $216 \pm 20$   $^\circ\text{C}$  with the sample in Fig. 8a and  $206 \pm 20$   $^\circ\text{C}$  with that in Fig. 8b. We hypothesize that the conditions under which the samples were analyzed may have varied slightly, resulting in the slightly different temperatures in each sample (albeit within our measurement uncertainty) and that the transformation process may be very sensitive to temperature at around 200  $^\circ\text{C}$ . This wide variation in outcomes suggests that the results of long duration Raman analysis with high laser power on small grains in aerogel need to be interpreted with caution. The presence of peaks associated with magnetite is indicative of the presence of that mineral in the original sample, but the strength of the peaks

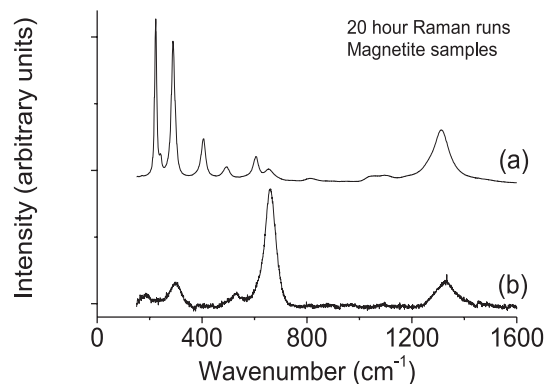
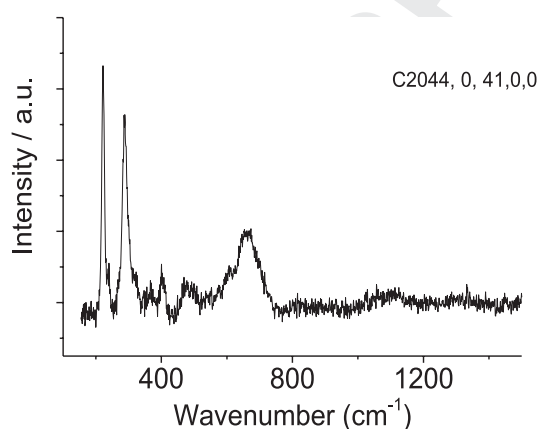


Fig. 8. Raman spectra from magnetite grains fired into aerogel at 6 km/s. The laser illumination was at full power for 20 h. Two grains were used. Before these long runs, the grains, when illuminated for short periods at lower laser intensity, gave magnetite spectra similar to that in Fig. 5. After the 20 h illumination, grain (a) is now mostly showing the spectrum associated with hematite, with weak magnetite peaks, whereas the spectrum for grain (b) is still dominated by the peaks from the original magnetite spectrum.

1 does not necessarily indicate the abundance of magne-  
 2 tite that was originally present. Any hematite peaks  
 3 from a long duration analysis could be interpreted as  
 4 due to heating and partial alteration during the Raman  
 5 analysis, rather than necessarily being indicative of the  
 6 presence of hematite pre-analysis.

#### 8 *Track slice C2044,0,41,0,0*

9 The slice of Stardust track C2044,0,41,0,0 was  
 10 examined optically and around the wall of the cavity  
 11 several grains in the size range 5–10  $\mu\text{m}$  were identified.  
 12 Most gave no Raman signal (with laser power attenu-  
 13 ated by the 8% filter to avoid any risk of damaging the  
 14 sample), but one (shown arrowed in Figs. 2 and 11) did.  
 15 To obtain a better signal to noise ratio in the spectra,  
 16 this sample was illuminated at full laser power (10 mW)  
 17 for 15 h. During this run, a full Stokes and anti-Stokes  
 18 spectrum was obtained and the sample temperature dur-  
 19 ing analysis was estimated as  $209 \pm 20$  °C. The result-  
 20 ing Raman spectrum is shown in Fig. 9 with peak  
 21 positions and widths given in Table 3. The spectrum is  
 22 very similar to that from the hematite grains that did  
 23 not undergo long duration analysis. The low wave shift  
 24 number peaks are present, although the peak in the  
 25 standard raw grains at just above 1300/cm is not totally  
 26 distinct above the background. We can also see that the  
 27 structure at just above 600/cm contains two peaks; one  
 28 at  $\sim 610$ /cm is compatible with the hematite standard  
 29 spectra, but the other at  $\sim 630$ /cm is similar to that  
 30 found in magnetite. The lack of a peak above 1300/cm  
 31 is not explained – as it is expected if hematite is present –  
 32 but apart from this discrepancy, the best explanation of  
 33 the spectrum is a combination of hematite and magne-  
 34



35  
36  
37  
38  
39  
40  
41  
42  
43  
44  
45  
46  
47  
48  
49  
50 Fig. 9. Raman spectra from Stardust sample C2044,0,41,0,0  
 51 (track 41). The peak positions and widths are given in Table 3.  
 52 By comparison with Fig. 5 (and Table 2), it can be seen that  
 53 peaks characteristic of both magnetite and hematite are pres-  
 54 ent (with the exception of the absence of a peak at around  
 1300–1340/cm).

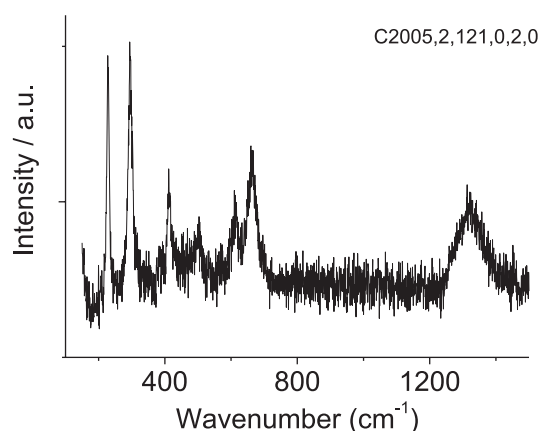
Table 3. Position and width of peaks in Raman shift spectra for Stardust samples.

Sample	Peak positions, width (/cm)
C2044,0,41,0,0	222.0, 8.3
	288.9, 19.5
	401.4, 16.2
	482.9, 31.8
	604.1, 59.7
C2005,2,121,0,2,0	664.1, 64.0
	228.3, 8.0
	295.5, 13.9
	413.5, 17.3
	612.4, 16.4
	663.1, 27.0
	1323.7, 102

tite (with the qualifications given above about the possi-  
 ble consequences of heat processing of magnetite grains  
 in aerogel as a result of long laser illumination at high  
 powers). This is discussed further below.

#### Terminal samples C2005,2,121,2,0 and C2005,2,121,1,0

Raman spectra were taken from one of the terminal  
 grains in track 121 (C2005, 2, 121, 2, 0) and an example  
 is shown in Fig. 10 (peak positions and widths are given  
 in Table 3). Laser power was 8–44% of the total (0.8–  
 4.4 mW), with illumination for 8 min in total on any  
 one grain. At wave numbers up to just above 600/cm,  
 the peaks typical of hematite were all visible. However,  
 above this, the two peaks indicative of magnetite were  
 also visible in the same spectrum. The peak at 663/cm



51  
52  
53  
54  
55 Fig. 10. Raman spectra from Stardust sample  
 C2005,2,121,0,2,0 (a track 121 sample). The peak positions  
 and widths are given in Table 3. By comparison with Fig. 5  
 (and Table 2), it can be seen that peaks characteristic of both  
 magnetite and hematite are present.

1 is clearly distinct from the hematite standard peak at  
 2 612/cm but agrees well with that for magnetite. Also,  
 3 the peak at 1324/cm has a peak position that is too  
 4 high a peak position and is too broad to be associated  
 5 with that in the standard hematite spectrum, but  
 6 matches better with the magnetite standard. The best  
 7 interpretation of the spectra is thus again a mixture of  
 8 hematite and magnetite. The laser-induced heating  
 9 effects in these samples were small; it was difficult to  
 10 identify the anti-Stokes lines above the background  
 11 noise level and we thus find that the sample tempera-  
 12 tures during the Raman analysis were  $\leq 87$  °C.

13 Sample C2005,2,121,1,0 analyzed at the OU Raman  
 14 gave no Raman signature of mineral structures. This is  
 15 consistent with the amorphous nature of this Fe oxide  
 16 as determined by electron diffraction.

### 17 X-ray Microfocus Spectroscopy – XRF and XANES-EX- 18 AFS of Track 41

19  
 20  
 21 The track 41 slice was found to contain a range of  
 22 different minerals and oxidation states. The grains are  
 23 scattered around the track's bulb margin. X-ray Spec-  
 24 trometry (Fig. 11) showed Fe hotspots, Fe-Ni com-  
 25 pounds, Fe-Ti (oxide – e.g., ilmenite), Cr-Fe-V-Ti-Mn  
 26 (oxide-chromite), and an unidentified Fe-Zn compound  
 27 (which may well be an aerogel contaminant, see below).  
 28 Chromite has previously been identified in Wild 2 mate-  
 29 rial e.g., in Al foil crater residues (Bridges et al. 2007).  
 30 The detectable presence of V and relatively high Ti con-  
 31 tents in the chromite are significant because this is char-  
 32 acteristic of extraterrestrial (chondritic) chromite rather  
 33 than terrestrial chromite (Alwmark and Schmitz 2006).  
 34 In this sample the chromite and Fe-Ti oxide were  
 35 adjacent grains (Fig. 11).

36 Fe-XANES analyses (Figs. 12a–c) show that Fe  
 37 hotspots have a marked absorption peak at 7110–  
 38 7111 eV, before the main K edge. Another peak associ-  
 39 ated with ferric oxide occurs at around 7185 eV  
 40 (Fig. 12b). Similar effects have been reported elsewhere  
 41 for ferric oxide-bearing phases e.g., Prietzel et al. (2007).  
 42 This pattern effectively rules out pyrrhotite and olivine  
 43 as the mineral identities. The Fe hotspot patterns are  
 44 very close to that of the magnetite (absorption peak at  
 45 7110 eV) and hematite standards (absorption peak at  
 46 7111 eV) and are consistent with a mixture of these 2  
 47 phases. To test this, we performed a simple fit between  
 48 standards and sample (Fig. 12c) over the Fe-XANES  
 49 edge and this suggests a mixture of 38% magnetite,  
 50 62% hematite in one of the sample grains. Fits to goe-  
 51 thite around its Fe K edge were much poorer confirm-  
 52 ing the absence of this mineral.

53 Sulfur could not be analyzed by XRF with the Ge  
 54 detectors but, by comparison with other work on Star-

dust samples (e.g., Leroux et al. 2008), it is possible that  
 sulfides could have been present. However, none of the  
 XANES-EXAFS spectra in track 41 grains are consist-  
 ent with an Fe-sulfide identity, sulfides being character-  
 ized by the absence of a marked absorption edge, e.g.,  
 pyrrhotite (Fig. 12c).

The Fe-Ni grain analyzed shows a marked absor-  
 bance feature around 7160 eV which distinguishes it  
 from the hematite-magnetite mixes. A similar absor-  
 bance feature was noted in Fe metal by Pingitore et al.  
 (2002). However, our sample also has an absorption  
 peak around 7111 eV, which is consistent with a mix-  
 ture of FeNi metal and ferric oxide. The Fe-Zn com-  
 pound also shows this absorbance feature showing that  
 it too has been oxidized to some extent.

## DISCUSSION

### Iron Oxides – Part of Comet Wild 2 or Relicts of Space Weathering, Terrestrial Contamination, Capture Heating and Analysis?

Irradiation of the comet's surface, the extreme thermal  
 processing of the cometary dust during capture, some heat-  
 ing during analysis and terrestrial contamination during  
 manufacture of the aerogel, all make interpretation of the  
 original cometary assemblage difficult.

#### *Space weathering*

Space weathering in lunar soils and asteroidal sur-  
 faces is manifested by nanophase metallic Fe (e.g., Piet-  
 ers et al. 2000; Noble et al. 2007) within silicates.  
 Farnham and Schleicher (2005) showed that Wild 2  
 had a reddened reflectance spectrum which suggests  
 that space weathering has occurred on its surface. If  
 this space weathered material is present, mixed in  
 below the comet's surface and was carried by the jets  
 from inside the comet into the coma then some of the  
 nm-sized Fe-bearing particles e.g., in 121,1,0 might  
 have originated as space weathered material on Comet  
 Wild 2. However, the O-bearing nature of the Fe-rich  
 phases studied here requires that if space-weathered  
 material was present it has undergone subsequent oxi-  
 dation. The Fe-Ti and Fe-V-Mn-Ti-Cr oxide cannot  
 have been derived through space weathering and  
 instead we consider they are part of the original come-  
 tary mineral assemblage.

#### *Capture heating*

During capture at 6.1 km/s, the cometary grains  
 experienced substantial heating. After the first demon-  
 stration of capture of mineral grains at high speed in  
 aerogel (Tsou et al. 1988), several studies of the effect of  
 capture on mineral grains, quickly followed, including

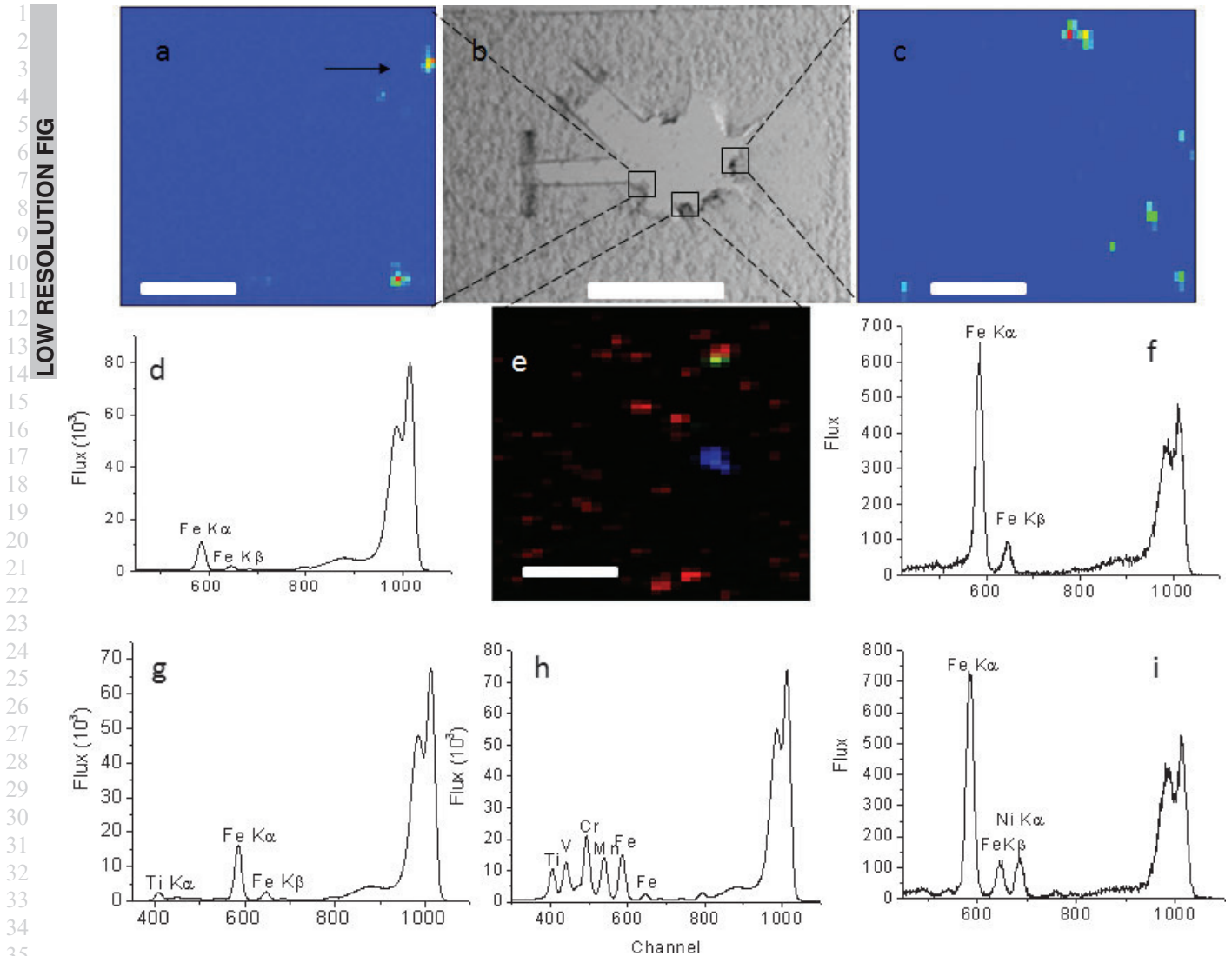


Fig. 11. XRS mapping of C2044,0,41 (track 41) using synchrotron X-rays. Note that the horizontal channel scale of the spectra does not correspond exactly to a keV scale although the relative positions of the characteristic peaks are accurate. (a) Reflected light microscope image of transverse slice of track 41. The central, roughly circular hole is the track cavity. The rectangular channels are artifacts made by the mounting forks used to hold the sample during extraction from the aerogel tile. The slice is 300  $\mu\text{m}$  thick. Scale bar is 1 mm. Mapped areas b–d and area with Raman analysis RM on hematite-magnetite grains shown. (b) Fe  $K\alpha$  map, each pixel measures approximately  $4 \times 4.5 \mu\text{m}$ , showing numerous grains approximately 10  $\mu\text{m}$  in diameter. Scale 80  $\mu\text{m}$ . The most commonly found spectra found at the Fe hotspots are shown in d, f. (c) Fe  $K\alpha$  map, which was also very similar to the Ni window (not shown here). Most hot spots in this area show a Fe-Ni-bearing composition displayed in i. (d) ‘Fe-hotspot’ spectra showing Fe  $K\alpha$  peak. The peak at channel no. 1000 is the scattering peak of the primary beam. (e) RGB intensity map of another position of Track 41, indicating Fe (red), Cr (green) and Zn (blue) hotspots. (f) Typical ‘Fe-hotspot’ spectra showing Fe  $K\alpha$  peaks. The peak at channel no. 1000 is the scattering peak of the primary beam. (g) Fe-Ti hotspot (ilmenite?) which is adjacent to the Fe-Cr-V-Ti-Mn hotspot. (h) Cr hotspot – V-rich chromite (green in RGB). The V intensity peak is greater than that of Ti. V enrichment is a characteristic of extraterrestrial chromite (i) Typical Fe, Ni spectrum from map c.

melting at grain surfaces, (e.g., Bunch et al. 1991; Barrett et al. 1992) and these are summarized in Burchell et al. (2006a,b). More recent studies include Noguchi et al. (2007), Hörz et al. (2008) and Burchell et al. (2008). It is clear from the abundant melted, rounded Fe sulfide and metal grains found along the tracks that

melting and sulfur remobilisation has occurred in general. This can be seen for example, in the work of Leroux et al. 2008, who, as here, examined grains from track 41, along with grains from track 35 (a Type B, bulbous track), and track 44 (a large feature where the incident particle hit both aerogel and the container wall)

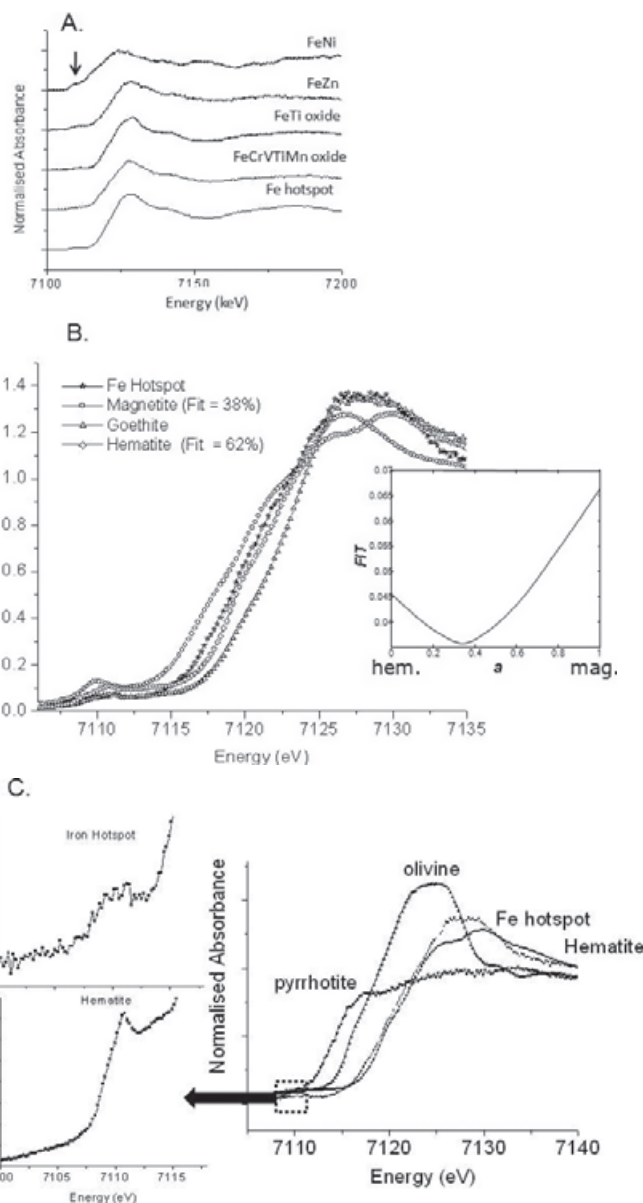


Fig. 12. Fe-XANES of minerals in track 41 and standards. 0.2–0.4 eV energy steps. (a) Fe-bearing phases within track 41. A **17** small absorbance feature around 7110–7112 eV (before the main absorption edges) is arrowed, which shows the presence of ferric oxide in all the samples, including the relict FeNi metal and the Fe-Zn contaminant phase. The relict FeNi metal also has an absorbance feature around 7160 eV, a feature characteristic of metal (Pingitore et al. 2002). (b) Comparison between goethite FeOOH, hematite Fe<sub>2</sub>O<sub>3</sub>, magnetite Fe<sub>2</sub>O<sub>3</sub>FeO standards with Fe hotspots. The main absorption edges (7115–7125 eV) have a similar gradient for all the samples and are consistent with the presence of ferric oxide. The inset diagram shows a best fit calculated between the two spectra – hematite and magnetite – that are most similar to the Fe hotspot spectra and are consistent with the microRaman data. Simple fit calculated by  $Fe - [(1-a)magnetite + a.hematite]$ . The typical Fe hotspot shown is fit as a mixture of 38% magnetite, 62% hematite. (c) Smaller energy range plotted to show the comparison between the Fe hotspot spectra and hematite. Plots (b) and (c) show that the Fe hotspot spectra are consistent with a mixture of magnetite and hematite and are not consistent with the presence of olivine or Fe sulfide (pyrrhotite). The olivine standard and Fe-sulfide standard both completely lack the peaks associated with ferric iron at 7110 eV and 7111 eV in magnetite, hematite, and the Fe hotspots.

and some grains of unknown track type. Recrystallised sulfide-metal assemblages frequently occur as metal (kamacite) cores and sulfide (pyrrhotite) rims in grains that range in size from nm to <100 nm diameter. Tae-

nite also occurs. Temperatures associated with capture of the cometary grains and metal-sulfide recrystallisation must have exceeded that of the Fe-Ni-S eutectic. This eutectic temperature increases with pressure and is at

1 least 950–1000 °C and gives a minimum temperature  
2 during capture.

3 There have been conflicting arguments for whether  
4 capture heating in aerogel causes oxidation or reduc-  
5 tion. Rietmeijer et al. (2008) described Fe silicides near  
6 the entrance of track 44: they suggested these resulted  
7 from the reduction of melted Fe-Ni sulfide grains. Mar-  
8 cus et al. (2008) also reported light-gas gun experiments  
9 where ferric iron had been reduced to ferrous com-  
10 pounds and considered that this was associated with  
11 capture heating in the presence of carbon within the  
12 aerogel. In contrast, Grossemy et al. (2008) used Fe-  
13 XANES to show that ferric iron-rich particles identified  
14 near the track mouth of Allende meteorite particle  
15 tracks in aerogel (shot with a light-gas gun) were the  
16 result of the oxidation of olivine. Fe-XANES spectra  
17 of FeNi metal suggests that some oxidation has  
18 occurred during capture heating within 1 mm of the  
19 track 41 entrance, in agreement with the conclusions of  
20 Grossemy et al. However, the relatively high abundance  
21 of magnetite within the Allende meteorite means that  
22 some of the magnetite in the Grossemy et al. experi-  
23 ments (and thus by analogy within our samples) might  
24 have been derived from the meteorite (or in our case  
25 comet Wild 2) rather than being due to capture-related  
26 oxidation of other minerals. Oxidation of FeNi metal  
27 after the samples were returned to Earth through inter-  
28 action with the atmosphere is also a possibility which  
29 cannot be ruled out as contributing to the limited oxida-  
30 tion identified in our Fe-XANES analyses of the Fe-Ni  
31 grains.

### 33 *Heating during analysis*

34 The Fe-XANES and Raman spectra obtained from  
35 grains in tracks 41 and 121 show evidence for mixtures  
36 of hematite and magnetite at scales < 3–5 µm spot size  
37 of the illumination laser in the Raman spectrometer  
38 and the synchrotron spot size. As discussed above,  
39 tests on the laboratory analogs showed that both  
40 hematite and magnetite remained distinct after capture  
41 in aerogel at speeds of ~6 km/s, but that prolonged  
42 exposure to strong laser illumination of magnetite  
43 grains in aerogel could produce hematite. This may  
44 have been relevant to just one of the grains which  
45 underwent a long duration analysis (Figs. 2 and 11) in  
46 the track 41 sample, but not to the extracted terminal  
47 grains from track 121 – both the magnetite-hematite  
48 mixtures and amorphous Fe oxide. We therefore sug-  
49 gest that, in most cases, the micron-scale hematite and  
50 magnetite grains are primordial cometary grains and  
51 are not artifacts of capture or analysis. We particularly  
52 also note that our XRS and Fe-XANES analyses iden-  
53 tified magnetite-hematite in spots that had not been  
54 analyzed at all by microRaman, so we do not believe

that the Raman analyses caused the formation of the  
observed Fe oxides.

### **Origin of the Fe Oxides**

Although we consider the Fe-Cr-V-Ti to be unam-  
biguously cometary in origin, the Fe oxide potentially  
has a more complex origin. Zn-bearing grains such as  
one identified in track 41 are a sign that there is some  
contamination from the manufacture of the aerogel (Zo-  
lensky, personal communication). As described above,  
we do not think that the Raman analyses formed the  
magnetite or amorphous Fe oxide, but it is possible that  
some of the hematite which partially replaces magnetite  
in a large grain in track 41 (Fig. 2) may be an analytical  
artifact. The Fe-XANES analyses suggest that capture  
heating in the aerogel has partially oxidized the outer  
parts of the FeNi metal grains. The intermixing of  
grains like Fe-Cr-V-Ti-Mn and Fe-Ti oxide around the  
track 41 slice with magnetite-hematite is consistent with  
the original cometary Fe-bearing oxides probably hav-  
ing been largely preserved. However, we do not yet have  
firm proof for the cometary origin of the hematite-mag-  
netite and further studies are required to check this.

The amorphous Fe oxide in sample 121,1,0 from  
track 121 could have originated through slight oxidation  
during capture of metallic iron. The origin of this amor-  
phous phase is uncertain and there is no firm evidence  
that it is not a terrestrial contaminant from aerogel  
manufacture, like the Zn-Fe compound in track 41.  
However, the 121,2,0 sample, also from track 121 does  
have a crystalline magnetite-hematite structure. Thus,  
the Fe oxides in tracks 41 and 121 have a variety of ori-  
gins mainly related to the Comet Wild 2 parent body  
and capture heating-oxidation with relatively minor  
effects from MicroRaman analyses and possible terres-  
trial contamination of amorphous Fe-oxide.

### **Comparisons to Chondrites and IDPs**

Iron oxide is found in IDPs (Rietmeijer 1998) inter-  
grown with phyllosilicates and is interpreted as having  
resulted from low temperature hydrothermal alteration  
on a cometary CI-like parent body (Keller et al. 1992)  
or other carbonaceous chondrite parent body. Rietmei-  
jer (1998) and Bradley et al. (1996) suggested that some  
magnetite found as overgrowths on silicate and sulfide  
minerals was the result of the heating and oxidation of  
silicates during atmospheric entry. Bradley (1994a)  
reported an Fe-Ni grain with a magnetite rim in an  
IDP. This was interpreted as having resulted from  
energetic particle bombardment during its passage in  
space. However, subsequent descriptions of space  
weathering effects have shown that this process is more

likely associated with reduction e.g., Noble et al. (2007). Zolensky and Lindstrom (1992) described magnetite in 12 chondritic IDPs. They suggested that magnetite around the outer margins of IDPs was formed by oxidation of the IDPs during atmospheric entry, but that magnetite within the centers of IDPs was primary.

Magnetite is present in CI, CV, oxidized CO, CM and CR chondrites. Keller et al. (1992), Brearley and Jones (1998) made the comparison between IDPs and CI chondrites because magnetite is one of the common signs of asteroidal alteration in this type of chondrite. Magnetite is the second most abundant phase in CI chondrites and has been described by Madsen et al. (1986), Morlok et al. (2006), Choi and Wasson (2003) and earlier work summarized in Brearley and Jones (1998). It occurs in a range of textures, but most commonly as 10–30  $\mu\text{m}$  size subspherical aggregates.  $\text{Fe}_2\text{O}_3$  as maghemite or hematite can also be present, although this could in turn be the product of magnetite oxidation (Haggerty and Baker 1967). CI magnetite is intergrown with phyllosilicates, particularly serpentine. If the magnetite now present in our Comet Wild 2 samples originated through such alteration, it might be expected to be associated with phyllosilicates such as serpentine minerals. The lack of phyllosilicates might be due to dehydration and recrystallisation during capture, although it remains an anomalous absence in the Wild 2 analyses to date. The composition of magnetite in CIs – like that identified in our C2005,2,121,1,0 sample – is essentially pure  $\text{Fe}_3\text{O}_4$  (Brearley and Jones 1998).

The asteroidal alteration in chondrites is believed to have occurred between 2 and 15 Myr after the formation of CAIs, but there does not appear to be any narrow set of oxygen fugacities or fluid composition associated with it (Zolensky et al. 2008). Morlok et al. (2006) concluded that low temperature alteration, including magnetite, in CIs formed in a closed system, where mineralogical differences in the lithologies reflected heterogeneities in the starting material. Although asteroidal alteration is one possible origin for magnetite in chondrite meteorites and IDPs the origin for the Wild 2 grains remains unclear.

Flynn (2008) used the result of 20 synchrotron analyses of tracks and fragments of tracks to suggest that the more volatile element abundances, e.g., Zn, Cu, showed an affinity to anhydrous porous IDPs but the more refractory elements, e.g., Ca to Fe, were closer to CI abundances. Thus, the Flynn analyses suggest there may be no easy, exclusive correlation between comet Wild 2 and either IDPs or CI chondrites. However, Ishii et al. (2008) noted that amorphous silicates with embedded metal and sulfide (known as GEMS) were a major constituent of anhydrous porous IDPs, but that the ini-

tial reports of these in comet Wild 2 samples were compatible with impact capture processing of the aerogel, rather than cometary GEMS of which there are currently no firm identifications in Wild 2. Furthermore, they noted that refractory minerals, CAIs, chondrules, and chondrule fragments are normally absent from, or exceedingly rare, in chondritic porous IDPs, but are found in almost all chondritic meteorites. Thus, Ishii et al. suggested that comet Wild-2 was most similar to chondritic material originating within the inner Solar System.

Our results show an unequilibrated mixture of reduced (e.g., FeNi metal) and oxidized phases in close proximity within the tracks. These phases can be present in both types of planetary material – chondrite and IDP. In IDPs, FeNi metal is often associated with GEMS (Bradley 1994a,b) although FeNi metal has also been identified in some asteroidal IDPs (Rietmeijer 2004). As discussed above, it has been suggested that GEMS are absent/not yet demonstrated in the Stardust samples. However, melted aerogel and its enclosed, rounded Fe-Ni-S grains can appear similar to GEMS, making identification difficult.

If the apparent absence of GEMS is genuine, then the Stardust samples including the Fe oxide ones studied here are most consistent with comet Wild-2 material being of a chondritic rather than IDP nature. However, more data are required from the Stardust samples before the origins of the different minerals including Fe oxides and the IDP versus chondritic analogies become clear.

## CONCLUSIONS

We have conducted a suite of materials characterisation analyses by Fe-XANES, TEM and microRaman on cometary dust grains captured by the NASA Stardust space mission soon after ejection from Comet 81P/Wild 2. This has been backed up by studies of analog samples created in light-gas gun experiments. We find:

1. We have identified iron oxides in a slice taken 0.8 mm along track 41 and some terminal samples from track 121. V-rich chromite (Fe-Cr-V-Ti-Mn oxide), Fe-Ti oxide (ilmenite?), and partially oxidized FeNi metal are present in track 41. The terminal samples from track 121 also contain traces of sulfide and Mg-rich silicate.
2. Fe oxide grains are either a magnetite-hematite mixture or have no structure detected by electron diffraction.
3. Fe-XANES shows that capture heating in the aerogel has led to partial oxidation of some phases, notably the FeNi metal. This does not appear to

1 have had a significant effect on the magnetite-hema-  
 2 tite. Our light-gas gun experiments on laboratory  
 3 analog samples of Wild 2 mineral analogs at  
 4 6 km/s suggest that the temperatures reached dur-  
 5 ing Raman analysis of many hours duration might  
 6 have been sufficient to cause some alteration of the  
 7 magnetite to hematite. However, apart potentially  
 8 from one large grain, which we analyzed for a long  
 9 time, we do not think our microRaman analyses  
 10 changed the mineralogy of the Fe oxides.

- 11 4. Amorphous Fe oxide might either be a product of  
 12 the capture-related or terrestrial atmospheric oxida-  
 13 tion of metallic iron. Terrestrial contamination  
 14 within the aerogel is also possible.
- 15 5. The oxides co-exist with reduced, metallic phases  
 16 (partially oxidized due to capture or terrestrial  
 17 alteration). This provides further evidence that this  
 18 comet consists of a diverse mixture of unequili-  
 19 brated mineral assemblages. Further work is required  
 20 to assess the similarities with IDP or chondrite sam-  
 21 ples and to calculate accurate abundances.
- 22 6. Finally, we recommend that, when reporting analy-  
 23 ses of Stardust samples, authors need to specify the  
 24 track and sample catalog numbers, and also state  
 25 the track type (A, B etc.) and where along the track  
 26 the sample grain(s) were located (wall of cavity, ter-  
 27 minal grain, etc.). This is necessary to help build up  
 28 a more consistent picture of the degree of (heat)  
 29 processing and mixing with aerogel that has  
 30 occurred during the capture event and the relation  
 31 of the analyzed grains to the original cometary dust  
 32 particle.

33  
 34 *Acknowledgments*—We thank the NASA Curatorial  
 35 Facility for supplying the Stardust samples used in this  
 36 work and preparing the terminal particles from track  
 37 121. Andrew Westphal and Christopher Snead of Uni-  
 38 versity of California (Berkeley) are thanked for prepar-  
 39 ing track 41 and providing track images. Matthew  
 40 Marcus, Sirine Fakra, and Andrew Westphal are also  
 41 thanked for giving access to their Berkeley XANES  
 42 mineral spectral database. This work was carried out  
 43 with the support of the Diamond Light Source. Fred  
 44 Mosselmans and Paul Quinn of Diamond are thanked  
 45 for assistance with collecting the microfocus spectro-  
 46 scopy data. Michael Cole (Univ. of Kent) is thanked for  
 47 operation of the light-gas gun. STFC (UK) is thanked  
 48 for financial support and NJF thanks the University of  
 49 Kent Alumni for financial support. Adrian Brearley,  
 50 Frans Rietmeijer, Mike Zolensky, and an anonymous  
 51 reviewer are thanked for their comments which  
 52 improved the manuscript.

53  
 54 *Editorial Handling*—Dr. Adrian Brearley

## REFERENCES

- Alwmark C. and Schmitz B. 2006. Extraterrestrial chromite in the resurge deposits of the early Late Ordovician Lockne crater, Central Sweden. *Earth and Planetary Science Letters* 253:291–303.
- Barrett R. A., Zolensky M. E., Hörz F., Lindstrom D. J., and Gibson E. K. 1992. Suitability of silica aerogel as a capture medium for interplanetary dust. *Proceedings of the Lunar and Planetary Science* 22:203–212.
- Bradley J. P. 1994a. Nanometre scale mineralogy and petrography of fine-grained aggregates in anhydrous interplanetary dust particles. *Geochimica et Cosmochimica Acta* 58:2123–2134.
- Bradley J. P. 1994b. Chemically anomalous, preaccretionally irradiated grains in interplanetary dust from comets. *Science* 265:925–929.
- Bradley J. P., Keller L. P., Brownlee D. E., and Thomas K. L. 1996. Reflectance spectroscopy of interplanetary dust particles. *Meteoritics & Planetary Science* 31:394–402.
- Brearley A. J. and Jones R. H. 1998. ??????. In *Planetary materials*, edited by Papike J. Washington, D.C.: Mineralogical Society of America. pp. 3–13–398. **11**
- Bridges J. C., Franchi I. A., and Green S. F. 2007. Stardust Microcrater residue compositional groups (abstract #2180). 38th Lunar and Planetary Science Conference. CD-ROM.
- Brownlee D., Tsou P., Aléon J., Alexander C. M. O'D., Araki T., Bajt S., Baratta G. A., Bastien R., Bland P., Bleuett P., Borg J., Bradley J. P., Brearley A., Brenker F., Brennan S., Bridges J. C., Browning N. D., Brucato J. R., Bullock E., Burchell M. J., Busemann H., Butterworth A., Chaussidon M., Chevroun  Chi M., Cintala M. J., Clark B. C., Clemett S. J., Cody G., Colangeli L., Cooper G., Cordier P., Daghlian C., Dai Z., d'Hendecourt L., Djouadi Z., Dominguez G., Duxbury T., Dworkin J. P., Ebel D. S., Economou T. E., Fakra S., Fairey S. A. J., Fallon S., Ferrini G., Ferroir T., Fleckenstein H., Floss C., Flynn G., Franchi I. A., Fries M., Gainsforth Z., Gallien J.-P., Genge M., Gilles M. K., Gillet P., Gilmour J., Glavin **12** D. P., Gounelle M., Grady M. M., Graham G. A., Grant P. G., Green S. F., Grossemy F., Grossman L., Grossman J. N., Guan Y., Hagiya K., Harvey R., Heck P., Herzog G. F., Hoppe P., Hörz F., Huth J., Hutcheon I. D., Ignatyev K., Ishii H., Ito M., Jacob D., Jacobsen C., Jacobsen S., Jones S., Joswiak D., Jurewicz A., Kearsley A. T., Keller L. P., Khodja H., Kilcoyne A. L. D., Kissel J., Krot A., Langenhorst F., Lanzirrotti A., Le L., Leshin L. A., Leitner J., Lemelle L., Leroux H., Liu M.-C., Luening K., Lyon I., MacPherson G., Marcus M. A., Marhas K., Marty B., Matrajt G., McKeegan K., Meibom A., Mennella V., Messenger K., Messenger S., Mikouchi T., Mostefaoui S., Nakamura T., Nakano T., Newville M., Nittler L. R., Ohnishi I., Ohsumi K., Okudaira K., Papanastassiou D. A., Palma R., Palumbo M. E., Pepin R. O., Perkins D., Perronnet M., Pianetta P., Rao W., Rietmeijer F. J. M., Robert F., Rost D., Rotundi A., Ryan R., Sandford S. A., Schwandt C. S., Schlutter D., Sheffield-Parker J., Simionovici A., Simon S., Sitnitsky I., Snead C. J., Spencer M. K., Stadermann F. J., Steele A., Stephan T., Stroud R., Susini J., Sutton S. R., Suzuki Y., Taheri M., Taylor S., Teslich N., Tomeoka K., Tomioka N., Toppani A., Trigo-Rodríguez J. M., Troadec D., Tsuchiyama A., Tuzzolino A. J., Tyliszczak T., Uesugi K., Velbel M., Vellinga J., Vicenzi E., Vincze L., Warren J., Weber I.,

- Weisberg M., Westphal A. J., Wirick S., Wooden D., Wopenka B., Wozniakiewicz P., Wright I., Yabuta H., Yano H., Young E. D., Zare R. N., Zega T., Ziegler K., Zimmermann L., Zinner E., and Zolensky M. 2006. Comet 81P/Wild 2 under a microscope. *Science* 314:1711–1716.
- Bunch T. E., Schultz P., Cassen P., Brownlee D., Pdalak M., Lissauer J., Reynolds R., and Chang S. 1991. Are some chondrule rims formed by impact processes? Observations and experiments. *Icarus* 91:76–92.
- Burchell M. J. and Kearsley A. T. 2009. Short period jupiter family comets after stardust. *Planetary and Space Science* 57:1146–1161.
- Burchell M. J., Cole M. J., McDonnell J. A. M., and Zarnecki J. C. 1999. Hypervelocity impact studies using the 2 MV Van de Graaff accelerator and two-stage light gas gun of the University of Kent at Canterbury. *Measurement Science Technology* 10:41–50.
- Burchell M. J., Creighton J. A., Cole M. J., Mann J., and Kearsley A. T. 2001. Capture of particles in hypervelocity impacts in aerogel. *Meteoritics & Planetary Science* 36:209–221.
- Burchell M. J., Graham G., and Kearsley A. 2006a. Cosmic dust collection in aerogel. *Annual Reviews of Earth and Planetary Science* 34:385–418.
- Burchell M. J., Mann J., Creighton J. A., Kearsley A. T., Graham G., and Franchi I. A. 2006b. Identification of minerals and meteoritic materials via Raman techniques after capture in hypervelocity impacts on aerogel. *Meteoritics & Planetary Science* 41:217–232.
- Burchell M. J., Fairey S. A. J., Wozniakiewicz P., Brownlee D. E., Hörz F., Kearsley A. T., See T. H., Westphal A., Green S. F., and Trigo-Rodríguez J. M. 2008. Characteristics of cometary dust tracks in Stardust aerogel and laboratory calibrations. *Meteoritics & Planetary Science* 43:23–40.
- Burchell M. J., Fairey S. A. J., Foster N. J., and Cole M. J. 2009. Hypervelocity capture of particles in aerogel: dependence on aerogel properties. *Planetary and Space Science* 57:58–70.
- Changela H. G. and Bridges J. C. 2009. TEM study of alteration assemblages in the nakhlites: variation with burial depth on mars (abstract #2302). 40th Lunar and Planetary Science Conference. CD-ROM.
- Choi B.-G. and Wasson J. T. 2003. Microscale oxygen isotopic exchange and formation of magnetite in the Ningqiang anomalous carbonaceous chondrite. *Geochimica et Cosmochimica Acta* 67:4655–4660.
- de Faria D. L. A., Venâncio Silva S., and de Oliveira M. T. 1997. Raman microspectroscopy of some iron oxides and oxyhydroxides. *Journal of Raman Spectroscopy* 28:873–878.
- Farnham T. L. and Schleicher D. G. 2005. Physical and compositional studies of Comet 81P/Wild 2 at multiple apparitions. *Icarus* 173:533–558.
- Flynn G. J. 2008. Physical, chemical, and mineralogical properties of Comet 81P/Wild 2 particles collected by stardust. *Earth Moon and Planets* 102:447–459.
- Flynn G. J., Bleuet P., Borg J., Bradley J. P., Brenker F. E., Brennan S., Bridges J., Brownlee D. E., Bullock E. S., Burghammer M., Clark B. C., Dai Z. R., Daghlian C. P., Djouadi Z., Fakra S., Ferroir T., Floss C., Franchi I. A., Gainsforth Z., Gallien J.-P., Gillet P., Grant P. G., Graham G. A., Green S. F., Grossemey F., Heck P. R., Herzog G. F., Hoppe P., Hörz F., Huth J., Ignatyev K., Ishii H. A., Janssens K., Joswiak D., Kearsley A. T., Khodja H., Lanzirrotti A., Leitner J., Lemelle L., Leroux H., Luening K., MacPherson G. J., Marhas K. K., Marcus M. A., Matrajt G., Nakamura T., Nakamura-Messenger K., Nakano T., Newville M., Papanastassiou D. A., Pianetta P., Rao W., Riekel C., Rietmeijer F. J. M., Rost D., Schwandt C. S., Sheffield-Parker J., Simionovici A., Sitnitsky I., Snead C. J., Stadermann F. J., Stephan T., Stroud R. M., Susini J., Suzuki Y., Sutton S. R., Taylor S., Teslich N., Troadec D., Tsou P., Tsuchiyama A., Uesugi K., Vekemans B., Vincenzi E. P., Vincze L., Westphal A. J., Wozniakiewicz P., Zinner E., and Zolensky M. E. 2006. Elemental compositions of comet 81P/Wild 2 samples collected by Stardust. *Science* 314:1731–1735.
- Grossemey F., Borg J., Djouadi Z., Simionovici A., Lemelle L., Eichert D., Deboffe D., Westphal A. J., and Snead C. 2008. In-situ Fe XANES of extraterrestrial grains trapped in aerogel collectors: an analytical test for the interpretation of Stardust samples analyses. *Planetary and Space Science* 55:966–973.
- Haggerty S. E. and Baker I. 1967. The alteration of olivine in basaltic and associated lavas. Part I. High temperature alteration. *Contributions to Mineralogy and Petrology* 16:233–257.
- Hörz F., Bastien R., Borg J., Bradley J. P., Bridges J. C., Brownlee D. E., Burchell M. J., Chi M., Cintala M. J., Dai Z. R., Djouadi Z., Dominguez G., Economou T. E., Fairey S. A. J., Floss C., Franchi I. A., Graham G. A., Green S. F., Heck P., Hoppe P., Huth J., Ishii H., Kearsley A. T., Kissel J., Leitner J., Leroux H., Marhas K., Messenger K., Schwandt C. S., Snead C., Stadermann F. J., Stephan T., Stroud R., Teslich N., Trigo-Rodríguez J. M., Tuzzolino A. J., Troadec D., Tsou P., Warren J., Westphal A., Wozniakiewicz P., Wright I., and Zinner E. 2006. Impact features on Stardust: implications for Comet 81P/Wild 2 dust. *Science* 314:1716–1719.
- Hörz F., Cintala M. J., See T. H., and Nakamura-Messenger K. 2008. Impact experiments with Al<sub>2</sub>O<sub>3</sub> projectiles into aerogel (abstract #1391). 39th Lunar and Planetary Science Conference. CD-ROM.
- Ishii H. A., Bradley J. P., Dai Z. R., Chi M. F., Kearsley A. T., Burchell M. J., Browning N. D., and Molster F. 2008. Comparison of comet 81P/Wild 2 dust with interplanetary dust from comets. *Science* 319:447–450.
- Joswiak D. J., Brownlee D. E., and Matrajt G. 2008. Surprisingly high abundance of Na and Cr-rich calcic pyroxenes in stardust tracks (abstract #2177). 39th Lunar and Planetary Science Conference. CD-ROM.
- Kearsley A. T., Borg J., Graham G. A., Burchell M. J., Cole M. J., Leroux H., Bridges J. C., Hörz F., Wozniakiewicz P. J., Bland P. A., Bradley J. P., Dai Z. R., Teslich N., Westphal A., See T., Hoppe P., Heck P. R., Huth J., Stadermann F. J., Floss C., Marhas K., Zinner E., Stroud R., Stephan T., and Leitner J. 2008. Dust from comet Wild 2: interpreting particle size, shape, structure and composition from impact features on the Stardust aluminium foils. *Meteoritics & Planetary Science* 43:41–74.
- Keller L. P., Thomas K. L., and McKay D. S. 1992. An interplanetary dust particle with links to CI chondrites. *Geochimica et Cosmochimica Acta* 56:1409–1412.
- Leroux H., Rietmeijer F. J. M., Velbel M. A., Brearley A. J., Jacob D., Langenhorst F., Bridges J. C., Zega T. J., Stroud R. M., Cordier P., Harvey R. P., Lee M., Gounelle M., and Zolensky M. E. 2008. A TEM study of thermally modified comet 81P/Wild 2 dust particles by interaction

- with the aerogel matrix during the Stardust capture process. *Meteoritics & Planetary Science* 43:97–120.
- Madsen M. B., Mørup S., Costa T. V. V., Knudsen J. M., and Olsen M. 1986. Superparamagnetic component in the Orgueil meteorite and Mössbauer spectroscopy studies in applied magnetic fields. *Nature* 321:501–503.
- Marcus M. A., Fakra S., Westphal A. J., Snead C. J., Keller L. P., Kearsley A., and Burchell M. J. 2008. Smelting of Fe-bearing glass during hypervelocity capture in aerogel. *Meteoritics & Planetary Science* 43:87–96.
- Martin T. P., Merlin R., Huffman D. R., and Cardona M. 1977. Resonant two magnon Raman scattering in  $\alpha$ -Fe<sub>2</sub>O<sub>3</sub>. *Solid State Communications* 22:565–567.
- Massey M. J., Baier U., Merlin R., and Weber W. H. 1990. Effects of pressure and isotopic substitution on the Raman spectrum of  $\alpha$ -Fe<sub>2</sub>O<sub>3</sub>: identification of two-magnon scattering. *Physical Review B* 41:7822–7827.
- Morlok A., Bischoff A., Stephan T., Floss C., Zinner E., and Jessberger E. K. 2006. Brecciation and chemical heterogeneities of CI chondrites. *Geochimica et Cosmochimica Acta* 70:5371–5394.
- Nakamura T., Noguchi T., Tsuchiyama A., Ushikubo T., Kita N. T., Valley J. W., Zolensky M. E., Kakazu Y., Sakamoto K., Mashio E., Uesugi K., and Nakano T. 2008. Chondrule like objects in short-period Comet 81P/Wild 2. *Science* 321:1664–1667.
- Noble S. K., Pieters C. M., and Keller L. P. 2007. An experimental approach to understanding the optical effects of space weathering. *Icarus* 192:629–642.
- Noguchi T., Nakamura T., Okudaira K., Yano H., Sugita S., and Burchell M. J. 2007. Thermal alteration of hydrated minerals during hypervelocity capture to silica aerogel at the flyby speed of STARDUST. *Meteoritics & Planetary Science* 42:357–372.
- Pieters C. M., Taylor L. A., Noble S. K., Keller L. P., Hapke B., Morris R. V., Allen C. A., McKay D. S., and Wentworth S. 2000. Space weathering on airless bodies: resolving a mystery with lunar samples. *Meteoritics & Planetary Science* 35:1101–1107.
- Pingitore N. E., Iglesias A., Bruce A., Lytle F., and Wellington G. M. 2002. Valences of iron and copper in coral skeleton: X-ray absorption spectroscopy analysis. *Microchemical Journal* 71:205–210.
- Prietzl J., Thieme J., Eusterhues K., and Eichert D. 2007. Iron speciation in soils and soil aggregates by synchrotron-based X-ray microspectroscopy (XANES, mu-XANES). *European Journal of Soil Science* 58:1027–1041.
- Rietmeijer F. J. M. 1998. In *Planetary materials*, edited by Papike J. Washington, D.C.: *Mineralogical Society of America*. pp. 2–1–2–95.
- Rietmeijer F. J. M. 2004. First report of taenite in an asteroidal interplanetary dust particle: flash-heating simulates nebular dust evolution (abstract #1060). 35th Lunar and Planetary Science Conference. CD ROM.
- Rietmeijer F. J. M., Nakamura T., Tsuchiyama A., Uesugi K., and Nakano T. 2008. Origin and formation of iron-silicide phases in the aerogel of the Stardust mission. *Meteoritics & Planetary Science* 42:121–134.
- Shebanova O. N. and Lazor P. 2003. Raman study of magnetite (Fe<sub>3</sub>O<sub>4</sub>): laser induced thermal effects and oxidation. *Journal of Raman spectroscopy* 34:845–852.
- Trigo-Rodriguez J. M., Domínguez G., Burchell M. J., Hörz F., and Llorca J. 2008. Bulbous tracks arising from hypervelocity capture in aerogel. *Meteoritics & Planetary Science* 43:75–86.
- Tsou P., Brownlee D. E., Laurance M. E., Hrubesh L., and Albee A. 1988. Intact capture of hypervelocity micrometeoroid analogs. Proceedings, 19th Lunar and Planetary Science conference. pp. 1205–1206.
- Westphal A. J., Snead C., Borg J., Quirico E., Raynal P. I., Zolensky M. E., Ferrini G., Colangeli L., and Palumbo P. 2002. Small hypervelocity particles captured in aerogel collectors: location, extraction, handling and storage. *Meteoritics & Planetary Science* 37:855–865.
- Westphal A. J., Brownlee D. E., Butterworth A. L., Fakra S., Gainsforth Z., Joswiak D., Marcus M. A., Snead C. J., and Oglione R. C. 2008. Oxidation state of Fe in the Jupiter-family Comet Wild 2 (abstract #2133). 39th Lunar and Planetary Science Conference. CD-ROM.
- Zhou B. and He D. 2008. Raman spectrum of vanadium pentoxide from density-functional perturbation theory. *Journal of Raman Spectroscopy* 39:1475–1481.
- Zolensky M. E. and Lindstrom D. J. 1992. Mineralogy of 12 large “chondritic” interplanetary dust particles. *Proceedings of the 19th Lunar and Planetary Science Conference* 22:161–169.
- Zolensky M. E., Zega T. J., Yano H., Wirick S., Westphal A. J., Weisberg M. K., Weber I., Warren J. L., Velbel M. A., Tsuchiyama A., Tsou P., Toppani A., Tomioka N., Tomeoka K., Teslich N., Taheri M., Susini J., Stroud R., Stephan T., Stadermann F. J., Snead C. J., Simon S. B., Simionovici A., Rietmeijer F. J. M., Rao W., Perronnet M. C., Papanastassiou D. A., Okudaira K., Ohsumi K., Ohnishi I., Nakamura-Messenger K., Nakamura T., Mostefaoui S., Mikouchi T., Meibom A., Matrajt G., Marcus M. A., Leroux H., Lemelle L., Le L., Lanzirrotti A., Langenhorst F., Krot A. N., Keller L. P., Kearsley A. T., Joswiak D., Jacob D., Ishii H., Harvey R., Hagiya K., Grossman L., Grossman J. N., Graham G. A., Gounelle M., Gillet P., Genge M. J., Flynn G., Ferroir T., Fallon S., Ebel D. S., Dai Z. R., Cordier P., Clark B., Chi M., Butterworth A. L., Brownlee D. E., Bridges J. C., Brennan S., Brearley A., Bradley J. P., Bleuet P., Bland P. A., and Bastien R. 2006. Mineralogy and petrology of comet 81P/Wild 2 nucleus samples. *Science* 314:1735–1739.
- Zolensky M. E., Krot A. N., and Benedix G. 2008. Record of low-temperature alteration in asteroids. *Reviews of Mineralogy and Geochemistry* 68:429–462.

# Author Query Form

Journal:       MAPS

Article:       1005

Dear Author,

During the copy-editing of your paper, the following queries arose. Please respond to these by marking up your proofs with the necessary changes/additions. Please write your answers on the query sheet if there is insufficient space on the page proofs. Please write clearly and follow the conventions shown on the attached corrections sheet. If returning the proof by fax do not write too close to the paper's edge. Please remember that illegible mark-ups may delay publication.

Many thanks for your assistance.

Query reference	Query	Remarks
1	<b>AUTHOR: A running head short title was not supplied; please check if this one is suitable and, if not, please supply a short title of up to 40 characters that can be used instead.</b>	
2	<b>AUTHOR: Please provide author forenames in full in the author field.</b>	
3	<b>AUTHOR: Please check unit 'km/s'.</b>	
4	<b>AUTHOR: Zolensky et al. 2007 has not been included in the Reference List, please supply full publication details.</b>	
5	<b>AUTHOR: Please give manufacturer information for Olympus BX40 microscope: company name, town, state (if USA), and country.</b>	
6	<b>AUTHOR: Please give manufacturer information FEI Sirion Field Emission Gun SEM (FEG-SEM) and a Philips XL30 Environmental SEM: company name, town, state (if USA), and country.</b>	
7	<b>AUTHOR: Please give manufacturer information for FIB-SEM: company name, town, state (if USA), and country.</b>	
8	<b>AUTHOR: Please give manufacturer information for <i>Pyspline</i> software and <i>PyMCA</i> software: company name, town, state (if USA), and country.</b>	
9	<b>AUTHOR: Please provide physical figure 4.</b>	
10	<b>AUTHOR: Burchell et al. (2006) has been changed to Burchell et al. (2006a,b) so that this citation matches the Reference List. Please confirm that this is correct.</b>	
11	<b>AUTHOR: Please provide the document title for reference Brearley and Jones (1998).</b>	
12	<b>AUTHOR: Please check the initial of the author 'Gillet', here and at subsequent occurrences.</b>	
13	<b>AUTHOR: Please provide the document title, name of the publisher for reference Rietmeijer (1998).</b>	

14	<b>AUTHOR: Figure 1 has been saved at a low resolution of 164 dpi. Please resupply at 300 dpi. Check required artwork specifications at <a href="http://www.blackwellpublishing.com/authors/digill.asp">http://www.blackwellpublishing.com/authors/digill.asp</a></b>	
15	<b>AUTHOR: Figure 3 has been saved at a low resolution of 166 dpi. Please resupply at 300 dpi. Check required artwork specifications at <a href="http://www.blackwellpublishing.com/authors/digill.asp">http://www.blackwellpublishing.com/authors/digill.asp</a></b>	
16	<b>AUTHOR: Figure 11 has been saved at a low resolution of 120 dpi. Please resupply at 600 dpi. Check required artwork specifications at <a href="http://www.blackwellpublishing.com/authors/digill.asp">http://www.blackwellpublishing.com/authors/digill.asp</a></b>	
17	<b>AUTHOR: Figure 12 has been saved at a low resolution of 188 dpi. Please resupply at 600 dpi. Check required artwork specifications at <a href="http://www.blackwellpublishing.com/authors/digill.asp">http://www.blackwellpublishing.com/authors/digill.asp</a></b>	

# MARKED PROOF

## Please correct and return this set

Please use the proof correction marks shown below for all alterations and corrections. If you wish to return your proof by fax you should ensure that all amendments are written clearly in dark ink and are made well within the page margins.

<i>Instruction to printer</i>	<i>Textual mark</i>	<i>Marginal mark</i>
Leave unchanged	... under matter to remain	Ⓟ
Insert in text the matter indicated in the margin	∧	New matter followed by ∧ or ∧ <sup>Ⓢ</sup>
Delete	/ through single character, rule or underline or ┌───┐ through all characters to be deleted	Ⓞ or Ⓞ <sup>Ⓢ</sup>
Substitute character or substitute part of one or more word(s)	/ through letter or ┌───┐ through characters	new character / or new characters /
Change to italics	— under matter to be changed	↙
Change to capitals	≡ under matter to be changed	≡
Change to small capitals	≡ under matter to be changed	≡
Change to bold type	~ under matter to be changed	~
Change to bold italic	≈ under matter to be changed	≈
Change to lower case	Encircle matter to be changed	≡
Change italic to upright type	(As above)	⊕
Change bold to non-bold type	(As above)	⊖
Insert 'superior' character	/ through character or ∧ where required	Υ or Υ under character e.g. Υ or Υ
Insert 'inferior' character	(As above)	∧ over character e.g. ∧
Insert full stop	(As above)	⊙
Insert comma	(As above)	,
Insert single quotation marks	(As above)	Ƴ or ƴ and/or ƶ or Ʒ
Insert double quotation marks	(As above)	ƶ or Ʒ and/or Ʒ or ƶ
Insert hyphen	(As above)	⊥
Start new paragraph	┌	┌
No new paragraph	┐	┐
Transpose	└┐	└┐
Close up	linking ○ characters	Ⓞ
Insert or substitute space between characters or words	/ through character or ∧ where required	Υ
Reduce space between characters or words		↑